

# Dynamical Phase Transitions of Information Flow in Random Quantum Circuits

J.-Z. Zhuang,<sup>1,\*</sup> Y.-K. Wu,<sup>1,2</sup> and L.-M. Duan<sup>1,2,†</sup>

<sup>1</sup>Center for Quantum Information, Institute for Interdisciplinary Information Sciences, Tsinghua University, Beijing 100084, PR China

<sup>2</sup>Hefei National Laboratory, Hefei 230088, PR China

We study how the information flows in many-body dynamics governed by random quantum circuits and discover a rich set of dynamical phase transitions in this information flow. The phase transition points and their critical exponents are established across Clifford and Haar random circuits through finite-size scaling. The flow of both classical and quantum information, measured respectively by Holevo and coherent information, shows similar dynamical phase transition behaviors. We investigate how the phase transitions depend on the initial location of the information and the final probe region, and find ubiquitous behaviors in these transitions, revealing interesting properties about the information propagation and scrambling in this quantum many-body model. Our work underscores rich behaviors of the information flow in large systems with numerous phase transitions, thereby sheds new light on the understanding of quantum many-body dynamics.

**Introduction.** Information flow in a quantum many-body system usually accompanies the growth of quantum entanglement and drives the system toward thermalization [1]. Apart from being essential in understanding non-equilibrium many-body physics, quantum dynamics about the information flow is also closely related to black hole theory and quantum gravity through the AdS/CFT correspondence [2, 3]. Under short-range interactions, the propagation of information is limited in a light-cone structure governed by the Lieb-Robinson bound [4, 5]. On the other hand, in the long-time limit, quantum information scrambling [6, 7] will occur for generic chaotic quantum systems, such that information initially encoded in localized degrees of freedom will spread over the whole system and cannot be recovered by local operations [5, 8, 9]. However, the detailed process between these two extreme cases is less well-understood and involves rich phenomena like pre-thermalization [10], many-body localization [11, 12], and many-body scars [13, 14].

Here we study the information retrievable from a subsystem of an initially locally encoded system, whose temporal derivative manifests the information flow. We adopt the random quantum circuit ansatz as depicted in Fig. 1(a), which is widely used to capture universal quantum dynamics in a chaotic system without being exposed to the detailed Hamiltonian [15–19]. By considering the information flow as a function of system parameters, we uncover a spectrum of behaviors beyond the light-cone and scrambling dynamics. Specifically, the information flow undergoes sudden shifts and can be used to delineate phase boundaries as a function of time and other system parameters. Similar to how order parameters switch from zero to nonzero values across a phase boundary, it exhibits distinct behaviors as the ratio of evolution time  $t$  to the system size  $N$  goes across the critical points in the thermodynamic limit  $N \rightarrow \infty$ , thereby exhibiting dynamical phase transitions (DPTs). Note that there are various notions of DPT in the literatures [20]. The most widely used definition is based on the nonanalytical behavior of the Loschmidt echo in closed many-body systems under Hamiltonian evolution [21, 22], which is deeply connected to conventional partition functions. However, this definition has no direct counterpart in random unitary circuits. On the other hand, DPT is de-

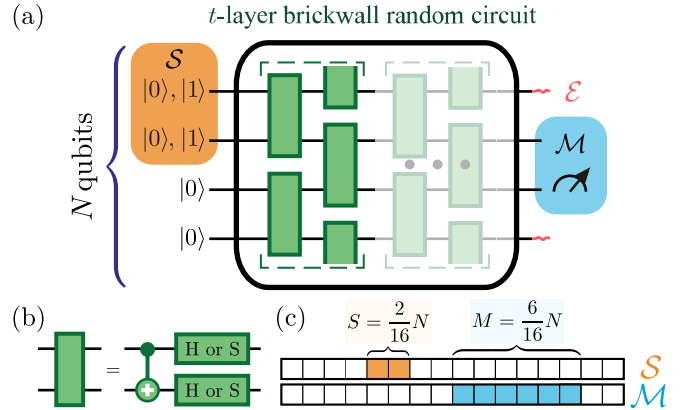


**FIG. 1.** Model for probing information dynamics. (a) Information is encoded into an  $S$ -qubit source in an  $N$ -qubit system with periodic boundary condition. Then after  $t$  layers of brick-wall-structured random circuits, we trace out the environment and retrieve the information from the remaining  $M$ -qubit measurement subsystem. Each “brick” (green rectangle) represents a random operation between the two nearby qubits. Here  $N = 4$  for illustration. (b) In each two-qubit random operation, we first apply a CNOT gate. Then independently for each qubit, we randomly apply a Hadamard or phase gate  $\text{diag}(1, e^{i\pi/2})$  with equal probability. (c) An example of source and measurement subsystem. For ease of expression, they are consecutively selected according to the 16 equal segments of the system.

finned differently in open quantum many-body systems [23, 24] and under the scenario of computational complexity [25].

Our key observation is the existence of dynamical phase transitions and their universality across both classical and quantum information, as well as within Clifford and Haar random circuits. We study their physical meanings by quantifying the DPTs’ positions and critical exponents using finite-size scaling. We study primarily the Clifford random circuits for the convenience of large-scale numerical simulation [26–28], and generalization is verified for generic quantum circuit ansatz [29, 30]. We also provide a general picture of informa-

tion propagation that applies to generic random circuit model setups. The discovery of such rich phase transition behavior sheds new light on the understanding of quantum many-body dynamics.

*Dynamical Phase Transitions in Information Flow.* Consider an  $N$ -qubit quantum system with periodic boundary condition, as shown in Fig. 1(a). We consecutively select  $S$  qubits as the source of information  $\mathcal{S}$  and  $M$  qubits as the measurement subsystem  $\mathcal{M}$ . We encode information into  $\mathcal{S}$ , apply a random circuit  $U$ , trace out the complement of  $\mathcal{M}$  as the environment  $\mathcal{E}$ , and retrieve the information from  $\mathcal{M}$ .

We first study the classical information dynamics in the quantum system, and the quantum information will be discussed later. We encode  $S$ -bits by preparing each qubit in  $\mathcal{S}$  into  $|0\rangle$  or  $|1\rangle$  with equal probability. The rest of the qubits are initialized as  $|0\rangle^{\otimes N-S}$ . We denote the set of all the  $2^S$  possible initial states as  $\{|\psi_i\rangle\}_{i=1}^{2^S}$ . After the random circuit, the extractable information can be quantified by the Holevo information

$$H(U) = S_{vn} \left( \sum_i p_i \rho_i^{\mathcal{M}} \right) - \sum_i p_i S_{vn}(\rho_i^{\mathcal{M}}) \quad (1)$$

where  $p_i = \frac{1}{2^S}$ ,  $\rho_i^{\mathcal{M}} = \text{Tr}_{\mathcal{E}}(U|\psi_i\rangle\langle\psi_i|U^\dagger)$  is the density matrix of  $U|\psi_i\rangle$  in  $\mathcal{M}$ ,  $S_{vn}$  denotes the von Neumann entropy.

The random circuit comprises  $t$  brick-wall layers, each corresponding to a unit of abstract time. Despite of stretched time scale, the structure of information dynamics is uniform across different probability distributions of the ‘‘bricks’’ over the Clifford group [31]. As illustrated in Fig. 1(b), we set each brick as a CNOT gate followed by random single-qubit Clifford gates. We denote  $\mathcal{U}_t$  as the set of all possible  $t$ -layered unitaries constructed in this way.

With fixed  $s = \frac{S}{N}$  and  $m = \frac{M}{N}$ , we study our system under increasing system sizes  $N$ . We numerically calculate the time evolution of average Holevo information  $H(t) = \frac{1}{|\mathcal{U}_t|} \sum_{U \in \mathcal{U}_t} H(U)$  and normalize it by  $h(t) = \frac{H(t)}{N}$ . The averaged value  $h(t)$  is sufficient to characterize each  $h(U)$  for generic  $U \in \mathcal{U}_t$  because, as we show in the Supplemental Material [31], its variance over  $\mathcal{U}_t$  vanishes in the large  $N$  limit. We also normalize the time by  $\tau = \frac{t}{N}$ .

As an representative example, we place a  $\frac{2N}{16}$ -qubit source inside a  $\frac{6N}{16}$ -qubit measurement subsystem. The information dynamics  $h(\tau)$  is shown in Fig. 2. In the limit of large  $N$ , three sharp turns of the curve can be observed, indicating discontinuous  $\partial_\tau h$  around the three points. Further verification that they are DPT points and their physical meanings will be discussed later. We denote them by their  $\tau$ -axis position  $\tau_e$  (escape),  $\tau_a$  (accelerate), and  $\tau_s$  (scrambled). At early times  $\tau < \tau_e$ ,  $h(\tau)$  keeps its initial value  $s$  because the light-cones starting from  $\mathcal{S}$  are still inside  $\mathcal{M}$ ; at  $\tau_e$ , information starts to decrease by escaping through the left boundary of  $\mathcal{M}$ ; when  $\tau = \tau_a$ , the rate of decreasing accelerates; after  $\tau > \tau_s$ , the system becomes scrambled  $h(\tau) = 0$ , consistent with its infinite-time limit [32].

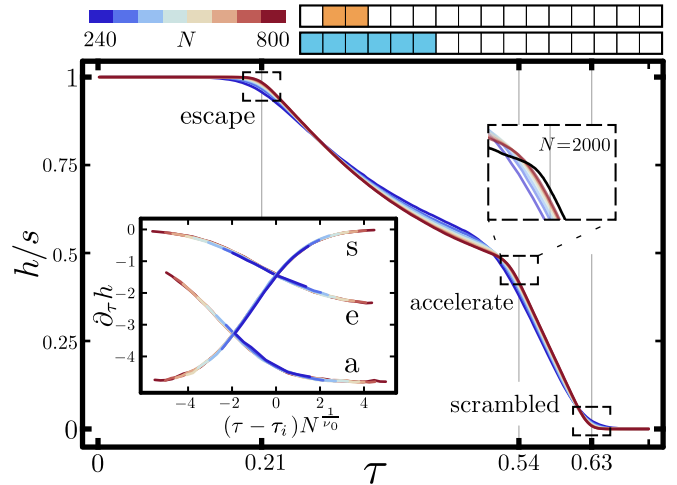


**FIG. 2.** Time evolution of average normalized Holevo information  $h(\tau)$  under eight system sizes from  $N = 240$  (blue) to  $N = 800$  (red). We fix  $s \equiv \frac{S}{N} = \frac{2}{16}$  and the measurement subsystem  $m \equiv \frac{M}{N} = \frac{6}{16}$ . At the three DPT points, the curve becomes sharp as  $N$  grows. We denote them from left to right as the  $\tau_e$ ,  $\tau_a$ , and  $\tau_s$  point. For the  $\tau_a$  point, we show an additional curve to illustrate its position. The inset further demonstrates the transition by finite-size scaling of  $\partial_\tau h$ . We find the critical exponent  $\nu_0 = 1.25$  and scale the  $\tau$ -axis near each of the three DPT points in the same way  $\tau'_i(\tau) = (\tau - \tau_i)N^{\frac{1}{\nu_0}}$  where  $i \in \{e, a, s\}$ . All of the eight curves collapse. Each data point in the inset is obtained from over  $6 \times 10^4$  samples.

To further verify and analyze the critical behavior, we perform finite-size scaling near each of the three DPT points  $\tau_i, i \in \{e, a, s\}$ . The curves  $\partial_\tau h$  of different system sizes  $N$  collapse when we scale the  $\tau$ -axis by the form  $\tau'_i(\tau) = (\tau - \tau_i)N^{\frac{1}{\nu_0}}$  where we find the critical exponent  $\nu_0$  to be equal for all  $i$ , as shown in the inset of Fig. 2. Thus, around each  $\tau_i$ , we can express  $\partial_\tau h$  of various  $N$  as a same function of  $\tau'_i$ . Then taking the thermodynamic limit  $N \rightarrow \infty$ , we verify the non-analyticity of information dynamics  $\partial_\tau h(\tau_i - 0) \neq \partial_\tau h(\tau_i + 0)$ . As will be discussed later, the critical exponent  $\nu_0$  is universal across various model configurations.

*DPTs' Positions and Physical Implications.* In order to determine the physical meanings of the three DPT points, we study how their positions can be determined by the selection of  $\mathcal{S}$  and  $\mathcal{M}$ . We begin by determining the  $\tau$ -axis positions of the escape point  $\tau_e$  and the scrambled point  $\tau_s$ , before discussing the accelerate point  $\tau_a$ .

With fixed  $s$  and  $m$ , we move  $\mathcal{S}$  from the middle to the boundary of  $\mathcal{M}$ , as shown in Fig. 3(a). By the periodic boundary condition, this only changes the relative position of  $\mathcal{S}$  and  $\mathcal{M}$ . We define the normalized distance  $l = \frac{L}{N}$  where  $L$  is the minimal distance from the qubits in  $\mathcal{S}$  to the boundaries of  $\mathcal{M}$ . When  $l$  decreases,  $\tau_e$  decreases linearly. When  $l = 0$ , the information can escape from  $\mathcal{M}$  at the first circuit layer,

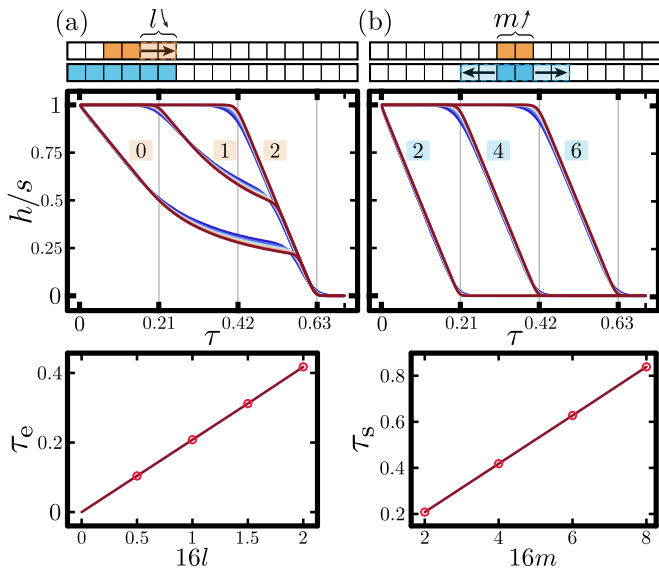


**FIG. 3.** Dynamics of  $h(\tau)$  under different selections of the source  $\mathcal{S}$  and the measurement subsystem  $\mathcal{M}$ . (a) We change the relative position between  $\mathcal{S}$  and  $\mathcal{M}$ . We keep  $\mathcal{S}$  inside  $\mathcal{M}$  and fix  $s = \frac{2}{16}$ ,  $m = \frac{6}{16}$ . Each group of curves is from various system sizes and labeled by the corresponding relative position  $16l$ , where  $l$  is the normalized distance between the right boundaries of  $\mathcal{S}$  and  $\mathcal{M}$ . The escape point's position  $\tau_e$  is proportional to  $l$ . The scrambled point  $\tau_s$  stays invariant. (b) We change  $\frac{2}{16} \leq m \leq \frac{1}{2}$  and fix  $\mathcal{S}$  in the middle of  $\mathcal{M}$ . Each group of curves is labeled by  $16m$ .  $\tau_s$  is proportional to  $m$ . For clarity, only part of the calculated  $h(\tau)$  curves are shown.

and the  $\tau_e$  point disappears at  $\tau = 0$  as expected. We have  $\tau_e(l) = l/v_e$ . The scrambled point  $\tau_s$ , which marks the transition from  $h > 0$  to  $h = 0$ , is independent of  $l$ . Such independence holds for any arbitrary selection of  $\mathcal{S}$  [31], as long as  $h(\tau)$  is not exponentially so that  $\tau_s$  does not vanish.

The scrambled point's position varies when  $m$  changes, as shown in Fig. 3(b) where we keep  $\mathcal{S}$  fixed within  $\mathcal{M}$ . For  $m < \frac{1}{2}$ , we observe a linear dependence  $\tau_s(m) = \frac{m}{2}/v_s$ . Combined with invariant  $\tau_s$  for arbitrary selections of  $\mathcal{S}$ , this implies that no information can be retrieved from any consecutive subsystem equal to or smaller than  $m$  after  $\tau_s$ . Non-consecutively selected subsystems of size  $m$  are also scrambled. One can see them scrambling faster by rearranging the qubits to make them consecutive and the resulting circuit would contain longer-range gates. We note that  $v_s$  can be directly connected with the entanglement velocity  $v_E$  [30], as demonstrated by the saturation of the entanglement entropy of  $\mathcal{M}$  to its maximum value at  $\tau_s$ .

We further found  $v_s = v_e \equiv v_I$  which we denote as the information velocity. The above analysis can be summarized as

$$\begin{cases} \tau_e(l) = l/v_I \\ \tau_s(m) = m/2v_I \end{cases} \quad (2)$$

which suggests a light-cone structure of information propagation underpinning both the  $\tau_e$  and  $\tau_s$  points.  $\tau_e$  is the moment when light-cones emitted from the qubits in  $\mathcal{S}$  reach the boundary of  $\mathcal{M}$ . Depending on whether they are exiting or entering  $\mathcal{M}$ , information starts to either decrease or increase. On the other hand,  $\tau_s$  is the moment when  $\mathcal{M}$  is entangled with  $M$  qubits, reflected by the light-cones emitted from  $\mathcal{M}$  covering  $2v_I t_s$  qubits outside of  $\mathcal{M}$ . To help understand the scrambling condition  $\frac{M}{M+2v_I t_s} \leq \frac{1}{2}$ , we note that this condition also applies when regarding the total  $M + 2v_I t_s$  qubits as a maximally entangled system [32]. Such picture is also applicable both when  $m > \frac{1}{2}$  and under the open boundary condition [31].

Though successful in predicting  $\tau_e$  and  $\tau_s$ , the light-cone picture cannot help understand the accelerate point  $\tau_a$ . Specifically, the  $\tau_a$  point is not “the time when light-cones start escaping from both ends of  $\mathcal{M}$ ”. For  $l = 0$  ( $l = \frac{1}{16}$ ) in Fig. 3(a), information can only reach the left boundary of  $\mathcal{M}$  at  $\tau = \frac{4}{16}/v_I$  ( $\tau = \frac{3}{16}/v_I$ ), later than the actual  $\tau_a$ . We further show that  $\tau_a$  has a nonlinear dependence on the model's length-scale [31], suggesting that all linear light-cone understandings are insufficient. Also, the accelerate point still exists when  $\mathcal{S}$  has no abrupt boundaries [31].

We have discussed above only  $m < \frac{1}{2}$ . For  $m > \frac{1}{2}$ , the  $\tau_e$  and  $\tau_s$  points still exist and are dominated by  $v_I$ . A major difference is that the  $\tau_a$  point does not exist and, after  $\tau_s$ , there are non-trivial dynamics followed by another DPT which we denote as  $\tau_r$  (recover).  $h$  reaches minimum at  $\tau_s$  and saturates to its non-zero infinite-time limit through  $\tau_r$  points. More details can be found in the Supplemental Material [31].

*Dynamics of Quantum Information.* Coherent information quantifies the reliably transmitted qubits through a noisy quantum channel. In quantum communication, it characterizes the quantum channel capacity when the encoding scheme is optimal [33, 34]. In quantum error correction, it upper bounds the number of qubits that can be recovered [35]. Using coherent information as a quantum counterpart of the Holevo information, we compare classical and quantum information dynamics.

We now study the quantum information flow with similar encoding scheme to that for the classical information. The only difference is that the initial state of the source would be an ensemble  $\rho^{\mathcal{S}} = (\frac{1}{2}I)^{\otimes S}$ . This is equivalent to mixing the pure states  $\{|\psi_i\rangle\}_{i=1}^{2^S}$  in the classical information model. Applying random circuit  $U$  and tracing out the environment  $\mathcal{E}$  form a quantum channel. The resulting coherent information  $C^{\mathcal{M}}$  can be calculated as [35, 36]

$$C^{\mathcal{M}} = S_{vn}(\rho^{\mathcal{M}}) - S_{vn}(\rho^{\mathcal{E}}) \quad (3)$$

where  $\rho^{\mathcal{M}} = \text{Tr}_{\mathcal{E}}(U(\rho^{\mathcal{S}} \otimes |0\rangle\langle 0|^{\otimes N-S})U^\dagger)$  is the density matrix of  $\mathcal{M}$ , and  $\rho^{\mathcal{E}}$  is similarly defined by exchanging  $\mathcal{E}$  and  $\mathcal{M}$ .

Like what we have done to the Holevo information, we average the coherent information over  $\mathcal{U}_t$  and define  $c = \frac{C^{\mathcal{M}}}{N}$ . We calculate  $c(\tau)$  for various positions of  $\mathcal{S}$  and  $\mathcal{M}$  with their

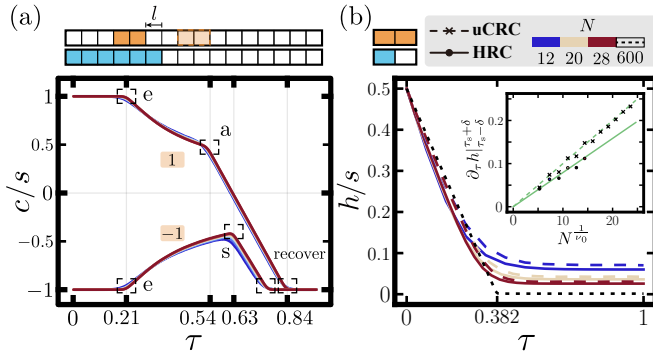


**FIG. 4.** Universality of DPT points in quantum circuit ansatz. (a) Dynamics of average normalized coherent information  $c(\tau)$ . We again specify  $s = \frac{2}{16}$  and  $m = \frac{6}{16}$ .  $\mathcal{S}$  is inside (outside) of  $\mathcal{M}$  with the boundary distance  $l = 1$  (denoted as  $l = -1$ ). For  $l = 1$ , up to three DPT points  $\tau_e$ ,  $\tau_a$ , and  $\tau_r$  can be observed. Additionally,  $c$  crosses from positive to negative at  $\tau_s$ . For  $l = -1$ , the  $\tau_a$  point does not exist and a DPT at  $\tau_s$  appears. (b) Information dynamics in Haar random circuits (HRC, solid line) and uniform sampling Clifford random circuits (uCRC, dashed line). Here, we set the system size from  $N = 12$  (blue) to  $N = 28$  (red) and fix  $s = 1$ ,  $m = \frac{1}{2}$ .  $h(\tau)$  in both systems exhibit similar behavior. The inset shows the scaling behavior of  $\partial_\tau h|_{\tau_s \pm \delta} \propto N^{\frac{1}{\nu_0}}$  under both HRC and uCRC where the same critical exponent  $\nu_0 = 1.25$  is applied.  $\tau_s$  is from the thermodynamic limit of uCRC and  $\delta = 0.012$  is a constant.

sizes  $s$  and  $m$  fixed.

As shown in Fig. 4(a), when  $\mathcal{S}$  is inside (outside) of  $\mathcal{M}$ ,  $c$  is initialized at its upper (lower) bound, indicating that all of the information are contained in  $\mathcal{M}$  (lost into  $\mathcal{E}$ ). The escape point's position  $\tau_e(l) = l/v_I$  is the same as that in the classical information model, verifying its physical meaning. For  $\mathcal{S}$  inside  $\mathcal{M}$ ,  $c$  turns from positive to negative at  $\tau_s$ , indicating that the amount of remaining quantum information turns to none. This is in agreement with the DPT point  $\tau_s$  in classical information dynamics.  $c$  converges to its infinite-time limit  $-s$  through the last DPT. Consistent with the classical model for  $m > \frac{1}{2}$ , we denote it as the  $\tau_r$  point.

We can understand the above phenomena in the context of private classical information transmission [36–38]. We encode classical information by  $\{|\psi_i\rangle\}_{i=1}^{2^S}$  and give a penalty of  $-1$  whenever one bit of information is leaked to and recoverable from the environment. The result  $C^{\mathcal{M}} = H^{\mathcal{M}} - H^{\mathcal{E}}$  is exactly the coherent information where  $H^{\mathcal{M}}$  and  $H^{\mathcal{E}}$  are the Holevo information in  $\mathcal{M}$  and  $\mathcal{E}$ , respectively. For  $\mathcal{S}$  outside of  $\mathcal{M}$ ,  $H^{\mathcal{M}}$  stays almost zero so that  $C^{\mathcal{M}} \approx -H^{\mathcal{E}}$ .  $H^{\mathcal{E}}$  stays at maximum until starts decreasing at the  $\tau_e$  point. At the scrambled point  $\tau_s$ ,  $H^{\mathcal{E}}$  reaches its minimum and starts recovering its value until saturation at the  $\tau_r$  point. With the size of  $\mathcal{E}$  satisfying  $\frac{N-M}{N} > \frac{1+s}{2}$ ,  $\mathcal{E}$  obtains all the  $S$ -bits after  $\tau_r$  while  $\mathcal{M}$  acquires no information.

One can also regard the random circuit here as the encoding

operation in QEC [39–41]. Tracing  $\mathcal{E}$  out would then correspond to the qubit loss error, and  $C^{\mathcal{M}}$  is the number of successfully preserved logical qubits. In our result for  $m < \frac{1}{2}$ , the information can never be perfectly recovered from  $\mathcal{M}$  as long as  $\mathcal{E}$  has non-zero overlap with  $\mathcal{S}$ , regardless of how deep the encoding circuit is. On the other side, we can study the case when  $m > \frac{1}{2}$  by exchanging  $\mathcal{E}$  and  $\mathcal{M}$  so that the qubits in  $\mathcal{M}$  instead of  $\mathcal{E}$  are lost. From  $C^{\mathcal{E}} = -C^{\mathcal{M}}$ , all the encoded quantum information can be recovered from  $\mathcal{E}$  at the  $\tau_r$  point. Our result gives the minimum and sufficient circuit depth for a perfect QEC recovery.

*DPTs in Haar random circuits.* To the best of our knowledge, existing methods – either analytical or numerical – are incapable of directly analyzing the information in large-scale Haar random circuit (HRC) systems. We will demonstrate that the DPT structure of information dynamics is universal across HRC and Clifford random circuits. Within the precision achievable with current methods, the critical exponent  $\nu_0$  of DPTs is also universal.

Specifically, we compare brick-wall circuits with two types of 2-qubit bricks: those generated from Haar random unitary, and those generated by uniformly sampling the Clifford group (uCRC), the latter being a unitary 2-design [42]. For an arbitrary pure initial state  $|\psi_i\rangle$ , the two circuits produce identical average purity of  $\mathcal{M}$  [30]. In order to reduce the finite-size drifts, we fix  $s = 1$ ,  $m = \frac{1}{2}$  which gives a simple information dynamics containing only one DPT point  $\tau_s$ .

As shown in Fig. 4(b),  $h(\tau)$  of HRC for small system sizes  $N \lesssim 28$  behave similarly to uCRC. We further demonstrate the universality of the critical exponent  $\nu_0 = 1.25$  in the inset. For fixed  $\delta$  satisfying  $\delta N^{\frac{1}{\nu_0}} \ll 1$ ,  $\partial_\tau h|_{\tau_s \pm \delta} \equiv \partial_\tau h(\tau_s + \delta) - \partial_\tau h(\tau_s - \delta)$  of uCRC should be proportional to  $N^{\frac{1}{\nu_0}}$ . This can be concluded from the collapsed  $\partial_\tau h(\tau')$  in the inset of Fig. 2 with non-zero slope near  $\tau' = 0$ . When applying to HRC the same  $\tau_s$  value from the thermodynamic limit of uCRC, the scaling behavior remains consistent  $\partial_\tau h|_{\tau_s \pm \delta} \propto N^{\frac{1}{\nu_0}}$ . More details can be found in the Supplemental Material [31].

*Discussions.* In summary, we have studied the dynamical phase transitions in information flow with universal behavior across random unitary circuits. We identified up to four DPT points in both classical and quantum information flow: escape, accelerate, scrambled, and recover. We studied their dependence on the model configuration, uncovering the light-cone structure of information propagation. The accelerate and recover points show new stages of propagation other than ballistic and scrambling behavior. The quantum circuit ansatz we focused on already encompasses a broad range of quantum systems. The potential for similar behavior in generic systems, especially those governed by Hamiltonian dynamics, remains an area of great interest. Although we discussed the DPTs only from the information perspective, we expect similar DPT behavior in other important physical quantities. The discovery of the DPTs shall thus shed new light on our understanding of generic quantum many-body dynamics.

**Acknowledgment:** We thank Z.-D. Liu and D. Yuan for



discussions. This work was supported by the Frontier Science Center for Quantum Information of the Ministry of Education of China and the Tsinghua University Initiative Scientific Research Program. The numerical calculations in this study were carried out on the ORISE Supercomputer.

\* zhuangjz21@mails.tsinghua.edu.cn

† lmduan@tsinghua.edu.cn

- [1] R. J. Lewis-Swan, A. Safavi-Naini, A. M. Kaufman, and A. M. Rey, Dynamics of quantum information, *Nat Rev Phys* **1**, 627 (2019).
- [2] D. Harlow, Jerusalem lectures on black holes and quantum information, *Rev. Mod. Phys.* **88**, 015002 (2016).
- [3] X.-L. Qi, Does gravity come from quantum information?, *Nature Phys* **14**, 984 (2018).
- [4] E. H. Lieb and D. W. Robinson, The finite group velocity of quantum spin systems, *Communications in Mathematical Physics* **28**, 251 (1972).
- [5] T. Rakovszky, S. Gopalakrishnan, S. A. Parameswaran, and F. Pollmann, Signatures of information scrambling in the dynamics of the entanglement spectrum, *Phys. Rev. B* **100**, 125115 (2019).
- [6] P. Hayden and J. Preskill, Black holes as mirrors: Quantum information in random subsystems, *J. High Energy Phys.* **2007** (9).
- [7] Y. Sekino and L. Susskind, Fast scramblers, *J. High Energy Phys.* **2008** (10), 065.
- [8] B. Swingle, Unscrambling the physics of out-of-time-order correlators, *Nature Phys* **14**, 988 (2018).
- [9] S. H. Shenker and D. Stanford, Black holes and the butterfly effect, *J. High Energy Phys.* **2014** (3), 67.
- [10] T. Mori, T. N. Ikeda, E. Kaminishi, and M. Ueda, Thermalization and prethermalization in isolated quantum systems: A theoretical overview, *J. Phys. B: At. Mol. Opt. Phys.* **51**, 112001 (2018).
- [11] D. A. Abanin, E. Altman, I. Bloch, and M. Serbyn, *Colloquium*: Many-body localization, thermalization, and entanglement, *Rev. Mod. Phys.* **91**, 021001 (2019).
- [12] A. Nico-Katz, Information-theoretic memory scaling in the many-body localization transition, *Phys. Rev. B* (2022).
- [13] C. J. Turner, A. A. Michailidis, D. A. Abanin, M. Serbyn, and Z. Papić, Weak ergodicity breaking from quantum many-body scars, *Nature Phys* **14**, 745 (2018).
- [14] D. Yuan, S.-Y. Zhang, Y. Wang, L.-M. Duan, and D.-L. Deng, Quantum information scrambling in quantum many-body scarred systems, *Phys. Rev. Research* **4**, 023095 (2022).
- [15] A. Chandran and C. R. Laumann, Semiclassical limit for the many-body localization transition, *Phys. Rev. B* **92**, 024301 (2015).
- [16] C. W. von Keyserlingk, T. Rakovszky, F. Pollmann, and S. L. Sondhi, Operator Hydrodynamics, OTOCs, and Entanglement Growth in Systems without Conservation Laws, *Phys. Rev. X* **8**, 021013 (2018).
- [17] T. Rakovszky, F. Pollmann, and C. W. Von Keyserlingk, Diffusive Hydrodynamics of Out-of-Time-Ordered Correlators with Charge Conservation, *Phys. Rev. X* **8**, 031058 (2018).
- [18] V. Khemani, A. Vishwanath, and D. A. Huse, Operator Spreading and the Emergence of Dissipative Hydrodynamics under Unitary Evolution with Conservation Laws, *Phys. Rev. X* **8**, 031057 (2018).
- [19] P.-Y. Chang, X. Chen, S. Gopalakrishnan, and J. H. Pixley, Evolution of Entanglement Spectra under Generic Quantum Dynamics, *Phys. Rev. Lett.* **123**, 190602 (2019).
- [20] M. Heyl, Dynamical quantum phase transitions: A review, *Rep. Prog. Phys.* **81**, 054001 (2018).
- [21] M. Heyl, A. Polkovnikov, and S. Kehrein, Dynamical Quantum Phase Transitions in the Transverse-Field Ising Model, *Phys. Rev. Lett.* **110**, 135704 (2013).
- [22] B. Žunkovič, M. Heyl, M. Knap, and A. Silva, Dynamical Quantum Phase Transitions in Spin Chains with Long-Range Interactions: Merging Different Concepts of Nonequilibrium Criticality, *Phys. Rev. Lett.* **120**, 130601 (2018).
- [23] C. Ates, B. Olmos, J. P. Garrahan, and I. Lesanovsky, Dynamical phases and intermittency of the dissipative quantum Ising model, *Phys. Rev. A* **85**, 043620 (2012).
- [24] J. P. Garrahan and I. Lesanovsky, Thermodynamics of Quantum Jump Trajectories, *Phys. Rev. Lett.* **104**, 160601 (2010).
- [25] A. Deshpande, B. Fefferman, M. C. Tran, M. Foss-Feig, and A. V. Gorshkov, Dynamical Phase Transitions in Sampling Complexity, *Phys. Rev. Lett.* (2018).
- [26] D. Gottesman, The Heisenberg Representation of Quantum Computers (1998), arxiv:quant-ph/9807006.
- [27] S. Aaronson and D. Gottesman, Improved simulation of stabilizer circuits, *Phys. Rev. A* **70**, 052328 (2004).
- [28] D. Fattal, T. S. Cubitt, Y. Yamamoto, S. Bravyi, and I. L. Chuang, Entanglement in the stabilizer formalism (2004), arxiv:quant-ph/0406168.
- [29] A. Nahum, J. Ruhman, S. Vijay, and J. Haah, Quantum Entanglement Growth Under Random Unitary Dynamics, *Phys. Rev. X* **7**, 031016 (2017).
- [30] A. Nahum, S. Vijay, and J. Haah, Operator Spreading in Random Unitary Circuits, *Phys. Rev. X* **8**, 021014 (2018).
- [31] See Supplemental Material at [URL will be inserted by publisher] for more details of classical information dynamics and the universality of DPTs in random quantum circuit ansatz.
- [32] J.-Z. Zhuang, Y.-K. Wu, and L.-M. Duan, Phase-transition-like behavior in information retrieval of a quantum scrambled random circuit system, *Phys. Rev. B* **106**, 144308 (2022).
- [33] H. Barnum, M. A. Nielsen, and B. Schumacher, Information transmission through a noisy quantum channel, *Phys. Rev. A* **57**, 4153 (1998).
- [34] A. S. Holevo and V. Giovannetti, Quantum channels and their entropic characteristics, *Rep. Prog. Phys.* **75**, 046001 (2012).
- [35] B. Schumacher and M. A. Nielsen, Quantum data processing and error correction, *Phys. Rev. A* **54**, 2629 (1996).
- [36] F. Leditzky, D. Leung, and G. Smith, Dephasing channel and superadditivity of coherent information, *Phys. Rev. Lett.* **121**, 160501 (2018).
- [37] I. Devetak, The Private Classical Capacity and Quantum Capacity of a Quantum Channel, *IEEE Trans. Inform. Theory* **51**, 44 (2005).
- [38] K. Li, A. Winter, X. Zou, and G. Guo, Private Capacity of Quantum Channels is Not Additive, *Phys. Rev. Lett.* **103**, 120501 (2009).
- [39] W. Brown and O. Fawzi, Short random circuits define good quantum error correcting codes, in *2013 IEEE Int. Symp. Inf. Theory* (IEEE, Istanbul, Turkey, 2013) pp. 346–350.
- [40] S. Choi, Y. Bao, X.-L. Qi, and E. Altman, Quantum Error Correction in Scrambling Dynamics and Measurement-Induced Phase Transition, *Phys. Rev. Lett.* **125**, 030505 (2020).
- [41] M. J. Gullans, S. Krastanov, D. A. Huse, L. Jiang, and S. T. Flammia, Quantum Coding with Low-Depth Random Circuits, *Phys. Rev. X* **11**, 031066 (2021).
- [42] H. Zhu, Multiqubit Clifford groups are unitary 3-designs, *Phys.*



# Supplemental Material for "Dynamical phase transition of information flow in random quantum circuits"

J.-Z. Zhuang,<sup>1,\*</sup> Y.-K. Wu,<sup>1,2</sup> and L.-M. Duan<sup>1,2,†</sup>

<sup>1</sup>Center for Quantum Information, Institute for Interdisciplinary Information Sciences, Tsinghua University, Beijing 100084, PR China  
<sup>2</sup>Hefei National Laboratory, Hefei 230088, PR China

We studied the dynamics of information in random quantum circuits and discovered dynamical phase transitions. In the main text, we consecutively select the information source  $\mathcal{S}$  and the measurement subsystem  $\mathcal{M}$ . Then we encode information into  $\mathcal{S}$ , apply a brick-wall-structured random circuit  $U \in \mathcal{U}_t$  and retrieve the information from  $\mathcal{M}$ . We probe the classical information dynamics by the normalized Holevo information  $h(U) = \frac{H(U)}{N}$ .

Here, we give additional details of the classical information dynamics, and discuss the universality of DPTs in various random quantum circuit models.

## SUPPLEMENTAL DETAILS OF CLASSICAL INFORMATION DYNAMICS

### Vanishing Variance of Normalized Holevo Information Under Large $N$ Limit

As mentioned in the main text, we only focused on the average value of information  $h(t) = \frac{1}{|\mathcal{U}_t|} \sum_{U \in \mathcal{U}_t} h(U)$  because it describes the behavior of each individual unitary in  $\mathcal{U}_t$  under the thermodynamic limit. Here, we show that the variance of  $\{h(U)|U \in \mathcal{U}_t\}$  converges to zero for all  $t$  when  $N \rightarrow \infty$ . We use the same model as in Fig. 2 in the main text and calculate the variance of  $h(U)$

$$\sigma^2(\tau) = \text{Var}_{U \in \mathcal{U}_t} h(U) \quad (\text{S1})$$

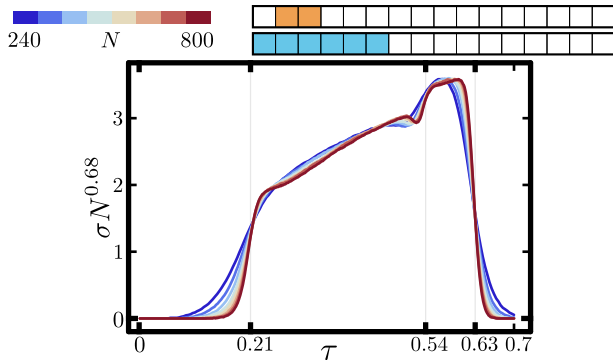


**FIG. S1.** Standard variance  $\sigma$  of the normalized Holevo information  $h(U)$  over random circuits  $U \in \mathcal{U}_t$ . The curves for different system sizes from  $N = 240$  (blue) to  $N = 800$  (red) approximately collapse when  $\sigma$  is scaled by  $N^{0.68}$ . The variance is calculated by over  $2 \times 10^4$  samples.

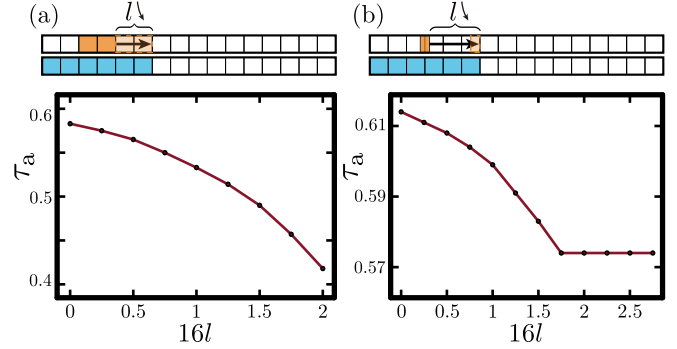


**FIG. S2.** The accelerate point's position  $\tau_a$  under different selections of the source  $\mathcal{S}$ .  $\mathcal{S}$  is moved from the middle towards the boundary of  $\mathcal{M}$ . The normalized distance from the right boundary of  $\mathcal{S}$  to that of  $\mathcal{M}$  satisfies  $\frac{m-s}{2} \geq l \geq 0$ . We fix  $m = \frac{6}{16}$ . (a) We set  $s = \frac{2}{16}$ . The accelerate point  $\tau_a$  decreases nonlinearly when  $l$  increases. (b) We set  $s = \frac{0.5}{16}$ . The accelerate point  $\tau_a$  decreases nonlinearly before saturation to a fixed value.

As shown in Fig. S1, we compute  $\sigma$  for various system sizes and found  $\sigma \sim N^{-0.68}$ . Thus,  $\sigma \rightarrow 0$  at the thermodynamic limit  $N \rightarrow \infty$ , so  $h(U)$  is the same for almost all  $U \in \mathcal{U}_t$ .

### Nonlinear Dependence of Accelerate Point $\tau_a$ on Length-scale

In the main text, we derived a light-cone picture by studying the  $\tau$ -axis position of the escape point  $\tau_e$  and the scrambled point  $\tau_s$ . However, the accelerate point  $\tau_a$  and the recover point  $\tau_r$  cannot be understood by the linear light-cone.

Here, we study how the accelerate point  $\tau_a$  depends on the selection of  $\mathcal{S}$  and  $\mathcal{M}$ . As shown in Fig. S2, when moving  $\mathcal{S}$  from the middle towards the boundary of  $\mathcal{M}$ ,  $\tau_a$  increases nonlinearly. Generally, the accelerate point occurs before the scrambled point  $\tau_a \leq \tau_s = \frac{m}{2v_1}$ . For smaller  $s$ , we also observe a saturation behavior  $\tau_a \geq \frac{m-s}{2v_1}$ .

### The Recover Point $\tau_r$

We discuss the information dynamics when  $m > \frac{s+1}{2}$ . Instead of becoming scrambled as in  $m < \frac{1}{2}$ , the information recovers its initial value at the long-time limit [S1]. As shown in Fig. S3(a), we set  $s = \frac{2}{16}$ ,  $m = \frac{10}{16}$  and fix the position of  $\mathcal{S}$  inside  $\mathcal{M}$ .  $h$  saturates to  $s$  through the recover point

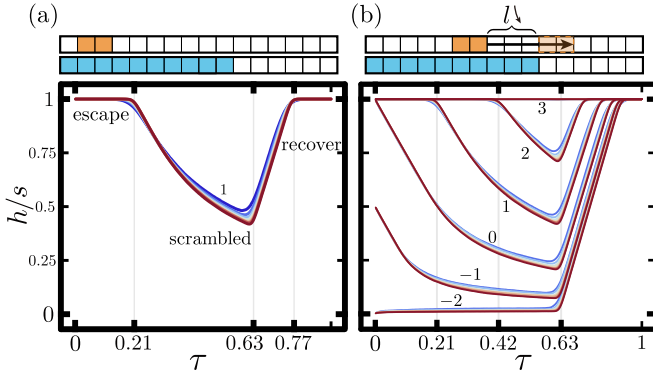


**FIG. S3.** Dynamics of  $h(\tau)$  under different selections of the source  $\mathcal{S}$  and the measurement subsystem  $\mathcal{M}$ . We set  $s = \frac{2}{16}$ ,  $m = \frac{10}{16} > \frac{1+s}{2}$ . (a) The position of  $\mathcal{S}$  and  $\mathcal{M}$  are fixed corresponding to  $l = \frac{1}{16}$  in (b). (b)  $\mathcal{S}$  is moved from the inside of  $\mathcal{M}$  to the outside, and the corresponding group of curves can be found from the top to bottom. Each group of curves is from various system sizes and labeled by the corresponding relative position  $16l$ , where  $l$  is the normalized distance from the right boundary of  $\mathcal{S}$  to that of  $\mathcal{M}$ . We set  $l$  negative when  $\mathcal{S}$  is not contained in  $\mathcal{M}$ .

$\tau_r$ . The whole propagation dynamics is as follows:  $h = s$  for  $0 < \tau < \tau_e$ . When the information propagates across the boundary of  $\mathcal{M}$  at  $\tau_e$ , information starts leaking out and  $h$  starts decreasing. Note that the minimal distance between boundaries of  $\mathcal{S}$  and  $\mathcal{M}$  is set to  $l = \frac{1}{16}$ , the same as that in Fig. 2. As the result,  $\tau_e$  is the same. At the scrambled point,  $h$  reaches its minimum. The position  $\tau_s = \frac{1-m}{2}/v_I$  is the same as in Fig. 2, where the measurement subsystem size is  $\frac{6}{16} = 1 - m$ .  $\mathcal{M}$  regains the information after  $\tau_s$  until the  $\tau_r$  (recover) point, where  $h$  saturates to its long-time limit. Combining with the  $\tau_a$  point shown in the main text, we found in total four different DPT points.

As shown in Fig. S3(b), we move  $\mathcal{S}$  from the inside of  $\mathcal{M}$  to the outside. Regardless of  $\mathcal{S}$ 's position, the  $\tau_s$  points share the same position  $\tau_s = \frac{1-m}{2}/v_I$ . In the main text, we introduced the information light-cone picture. For the complement of  $\mathcal{M}$  with size  $m' \equiv 1 - m < \frac{1}{2}$ ,  $\tau_s = \frac{m'}{2}/v_I$  is the moment when  $\mathcal{M}'$  is entangled with  $M'$  qubits, reflected by the light-cones emitted from  $\mathcal{M}'$  covering  $2v_I t_s$  qubits outside of  $\mathcal{M}'$ . Here, the scrambled point of  $\mathcal{M}$  shares the same  $\tau$ -axis position. At  $\tau_s$ , the number of qubits covered by the light-cones ceases to increase and saturates to  $N - M$ . Correspondingly, the information stops decreasing.

Though we found no method to infer the  $\tau_r$  point's position, there are some patterns that  $\tau_r$  shares with  $\tau_a$ . The  $\tau_r$  points always occur later than  $\tau_s$ . Moreover, as the relative position of  $\mathcal{S}$  and  $\mathcal{M}$  changes, the slope of the increasing  $h(\tau)$  between  $\tau_s$  and  $\tau_r$  is invariant. The slope of the decreasing  $h(\tau)$  between  $\tau_a$  and  $\tau_s$  in Fig. 3(a) is also invariant, but the two slopes are not equal.

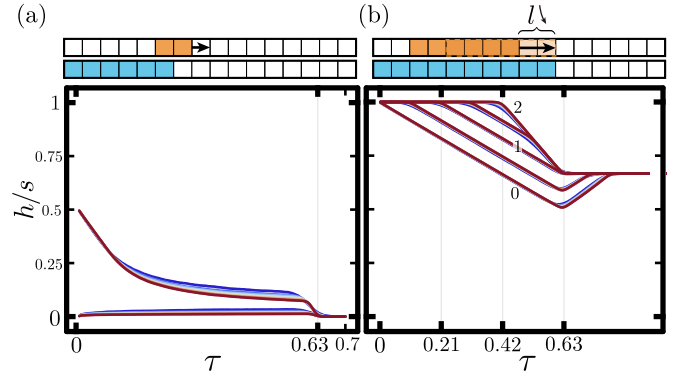


**FIG. S4.** Dynamics of  $h(\tau)$  under different selections of the source  $\mathcal{S}$  and the measurement subsystem  $\mathcal{M}$ . (a) We set  $s = \frac{2}{16}$  and  $m = \frac{6}{16}$ .  $\mathcal{S}$  is moved out of  $\mathcal{M}$ . (b) We set  $s = \frac{6}{16}$  and  $m = \frac{10}{16}$ . The measurement subsystem satisfies  $\frac{1}{2} < m < \frac{1+s}{2}$  so that the information  $0 < h(\tau \rightarrow \infty) < s$ . The normalized boundary-to-boundary distance  $l$  between  $\mathcal{S}$  and  $\mathcal{M}$  varies with each step  $\Delta l = 0.5$ .

#### More Consecutive Selections of $\mathcal{S}$ and $\mathcal{M}$

In the main text, for  $m < \frac{1}{2}$ , we showed the evolution of Holevo information when  $\mathcal{S}$  is contained in  $\mathcal{M}$ . Here, we study the case when  $\mathcal{S}$  is not contained in  $\mathcal{M}$ . As shown in Fig. S4(a), when  $\mathcal{S}$  is placed adjacent with  $\mathcal{M}$ ,  $h$  is initialized as 0. However, the information increases to a non-zero value for finite  $N$ . It converges to zero when  $N$  goes to infinity at a speed roughly  $\sim N^{-0.8}$ , much slower than the exponential convergence speed when scrambled  $\tau > \tau_s$ . This is in contrast with the case when  $\mathcal{S}$  is far away from  $\mathcal{M}$ , in which  $h(\tau)$  is exponentially small for all  $\tau$  because the information is scrambled before the light-cones reach  $\mathcal{M}$ . When half of  $\mathcal{S}$  is in  $\mathcal{M}$  and the other half is not,  $h$  is initialized at  $\frac{s}{2}$ . For both positions of  $\mathcal{S}$ , the  $\tau_s$  point is invariant as in Fig. 2.

We also show the information dynamics when  $\frac{1}{2} < m < \frac{s+1}{2}$ . See Fig. S4(b), we set  $s = \frac{6}{16}$  and  $m = \frac{10}{16}$ .  $\mathcal{S}$  is placed inside  $\mathcal{M}$  in the middle with the minimum distance between boundary  $l = \frac{1}{16}$ . The infinite-time limit of  $h(\tau)/s = (2m - 1)/s = \frac{2}{3}$ . As we move  $\mathcal{S}$  towards the boundary of  $\mathcal{M}$ , the DPT types changes from  $\tau_e$ ,  $\tau_a$  and  $\tau_s$  to  $\tau_e$ ,  $\tau_s$  and  $\tau_r$ . We conclude that  $\tau_a$  and  $\tau_r$  does not appear simultaneously for classical information propagation within our model. Similar to  $\tau_a$ ,  $\tau_r$  also has nonlinear dependence on the model's length-scale. Both of their positions are hard to predict. We classify them into two types because, as mentioned in the main text, they appear simultaneously for quantum information.

#### UNIVERSALITY OF DPTS IN RANDOM CIRCUIT ANSATZ

Under the encoding-decoding protocol and the random quantum circuit ansatz with brick-wall structure, we vary our model to verify the existence of DPTs and the universality of



their properties.

### Open Boundary Condition

With the same selection of  $S$  and  $\mathcal{M}$ , we compare the dynamics of  $h(\tau)$  under periodic and open boundary condition (P/O BC), see Fig. S5(a). Consistent with our intuition, open boundaries block the propagation of information. The information scrambles slower under OBC compared to PBC. However, this does not change the structure of the information dynamics. As long as  $\mathcal{M}$  remains consecutive under OBC, all the DPT points still exist with their physical meanings unchanged. Also, the critical exponent for all the DPTs remains the same  $\nu_0 = 1.25$ .

We place  $\mathcal{M}$  adjacent to the open boundary and fix  $m = \frac{6}{16}$ . We further found that the position of the scrambled point under OBC is exactly twice as that under PBC

$$\begin{aligned}\tau_s^{\text{OBC}} &= \frac{6}{16}/v_I \\ \tau_s^{\text{PBC}} &= \frac{m}{2}/v_I\end{aligned}$$

As shown in Fig. S5(a), after rescaling the  $\tau$ -axis for OBC by  $\tau' = \frac{1}{2}\tau$ , the scrambled point, as well as  $h(\tau)$  between  $\tau_a$  and  $\tau_s$ , coincides for P/O BC. This is in agreement with the physical picture of information propagation mentioned in the main text. Under PBC, the light-cones from  $\mathcal{M}$  propagates on both directions. Here, the light-cones are blocked on the left side, and it takes a doubled time for the region entangled with  $\mathcal{M}$  to grow and reach the size of  $\mathcal{M}$ . The halved increasing speed of the affected region also corresponds to the halved decreasing speed of information before  $\tau_s$ .

We can also gain insights into the position of the escape point  $\tau_e$  as follows. Under PBC, information escapes from the left side of  $\mathcal{M}$  at  $\tau_e^{\text{PBC}} = \frac{1}{16}/v_I$ . Under OBC, information can only escape from the right boundary of  $\mathcal{M}$ , which is three times the distance under PBC. In fact,  $\tau_e^{\text{OBC}} \approx \frac{3}{16}/v_I$  with  $\tau_e^{\text{OBC}}$  relatively 5% larger than  $3\tau_e^{\text{PBC}}$ . The discrepancy is likely due to the boundary effect because it extinguishes when  $S$  and  $\mathcal{M}$  are moved away from the boundary. In fact, when  $\mathcal{M}$  is moved one unit right (figure not shown), the decreasing speed before  $\tau_s^{\text{OBC}} = \frac{5}{16}/v_I$  is still halved and there is a DPT point at  $\tau_e^{\text{OBC}} = \frac{3}{16}/v_I$  as expected.

### Other random Clifford circuits

In the main text, each ‘‘brick’’ in the brick-wall-structured circuits represents a CNOT gate followed by, for each qubit, a random gate selected from the Hadamard gate and the phase gate  $\text{diag}(1, e^{i\pi/2})$  with equal probability. To verify the universality of DPTs over the choice of Clifford random circuits, we generate each ‘‘brick’’ by uniformly sampling the 2-qubit Clifford group (uCRC), as shown in Fig. S5(b). Though the  $\tau_a$  points’ positions deviates with each other by 1%, the critical

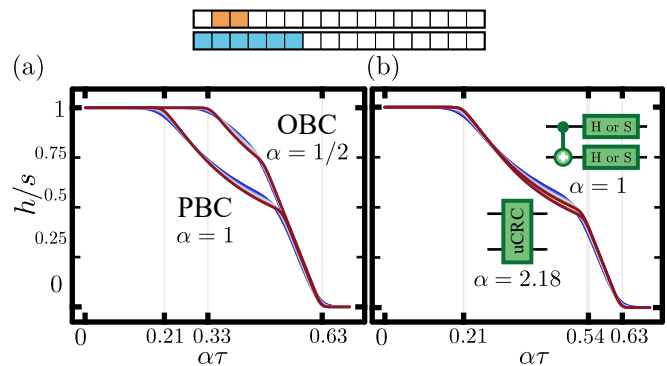


**FIG. S5.** We set  $s = \frac{2}{16}$ ,  $m = \frac{6}{16}$ . (a) We compare the information dynamics under periodic/open boundary condition. The  $\tau$ -axis for the latter is rescaled linearly by  $\alpha = \frac{1}{2}$ . (b) We compare the information dynamics with different random distributions of Clifford unitary. Specifically, each two-qubit random operation is generated by logic gates as in the main text or by sampling uniformly over 2-qubit Clifford group. For the latter, the  $\tau$ -axis is rescaled linearly by  $\alpha = 2.18$ . Though  $h(\tau)$  is different, the  $\tau_e$  and  $\tau_s$  points coincide.

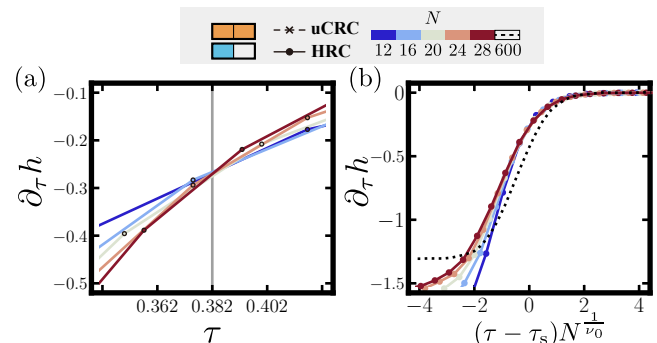


**FIG. S6.** Information dynamics in Haar random circuits (HRC, solid line). We compare it with that in uniform sampling Clifford random circuits (uCRC, dashed line). Here, we set the system size from  $N = 12$  (blue) to  $N = 28$  (red) and fix  $s = 1$ ,  $m = \frac{1}{2}$ . (a)  $\partial_\tau h$  for different  $N$  overlap with each other at a same point. This determines the DPT position at the crossing  $\tau_s = 0.382$ . The same value as the scrambled point of uCRC. (b) Finite-size scaling of  $\partial_\tau h$ . The  $\tau$  axis near  $\tau_s$  is scaled by  $\tau'_s(\tau) = (\tau - \tau_s)N^{\frac{1}{\nu_0}}$  where the critical exponent  $\nu_0 = 1.25$ . All of the five curves collapse.

exponents as well as the  $\tau_e$  and  $\tau_s$  positions are identical when we rescale the  $\tau$ -axis  $\tau' = \alpha\tau$  by the same factor  $\alpha$ . Thus, the choice of Clifford random circuits only affects the time scale of information propagation, rather than its overall structure.

### Haar random circuits

We next discuss the information dynamics in Haar random circuits (HRC). To the best of our knowledge, existing methods – either analytical or numerical – are incapable of directly analyzing the information in large-scale HRC systems. We will provide evidences that the information dynamics in HRC shares the same properties with that in uCRC.

Before numerical simulation results, we first undertake an analytical examination of the connection between HRC and uCRC. For a circuit  $U$  generated under the brick-wall structure, define  $\rho_i^{\mathcal{M}} = \text{Tr}_{\mathcal{E}}(U|\psi_i\rangle\langle\psi_i|U^\dagger)$  as the density matrix of  $\mathcal{M}$ . The average purity of  $\mathcal{M}$

$$\mathcal{P} = \text{Tr}(\rho_i^{\mathcal{M}})^2 \quad (\text{S2})$$

is identical [S2] for both circuits under arbitrary circuit depth of  $U$  and arbitrary pure initial state  $|\psi_i\rangle$ . Note that in uCRC, each ‘‘brick’’ sampling from the 2-qubit Clifford group forms a unitary 2-design. Recall that the Renyi- $\alpha$  entropy is defined by  $S_\alpha = \frac{1}{1-\alpha} \log_2 \text{Tr}(\rho_i^{\mathcal{M}})^\alpha$  whose  $\alpha \rightarrow 1$  limit equals the von Neumann entropy  $S_{vn} \equiv S_1$ . As a special case of von Neumann entropy’s generalization,  $S_2$  shares the same mathematical structure and many properties with  $S_1$  [S3]. The purity  $\mathcal{P}$  is directly related with  $S_2$  by

$$\mathcal{P} = 2^{-S_2} \quad (\text{S3})$$

This already ensures similar behavior of  $S_{vn}(\rho_i^{\mathcal{M}})$  contained in the second term of the Holevo information

$$H(U) = S_{vn}\left(\sum_i p_i \rho_i^{\mathcal{M}}\right) - \sum_i p_i S_{vn}(\rho_i^{\mathcal{M}}) \quad (\text{S4})$$

In summary, from the same average value of  $\mathcal{P}$ , the direct relation from  $\mathcal{P}$  to  $S_2$  and the similarity between  $S_1$  and  $S_2$ , we conclude the similarity of Holevo information dynamics between HRC and uCRC.

For  $h(\tau)$  under HRC, we can only simulate relatively small system sizes  $N \lesssim 28$ . In order to reduce the finite-size drifts, we fix  $s = 1, m = \frac{1}{2}$  which gives a simple information dynamics containing only one DPT point  $\tau_s$ , as illustrated in Fig. 4(b) in the main text. To verify that the  $\tau_s$  point’s position is equal for HRC and uCRC, we perform the same finite-size scaling for both systems. Fig. S6(a) shows  $\partial_\tau h$  for various  $N$ . The DPT position can be determined by the crossing  $\tau_s = 0.382$ , consistent with uCRC. Fig. S6(b) further demonstrates that the critical exponent in HRC is equal to that in uCRC  $\nu_0 = 1.25$ . When we scale the  $\tau$ -axis by the form  $\tau'_i(\tau) = (\tau - \tau_s)N^{\frac{1}{\nu_0}}$ ,  $\partial_\tau h$  of different system sizes  $N$  collapse near  $\tau' = 0$ .

#### Independence of DPTs on the $\mathcal{S}$ ’s boundary

In the main text, our consecutive selection of  $\mathcal{S}$  creates abrupt boundaries on both sides. Here, we consider how the

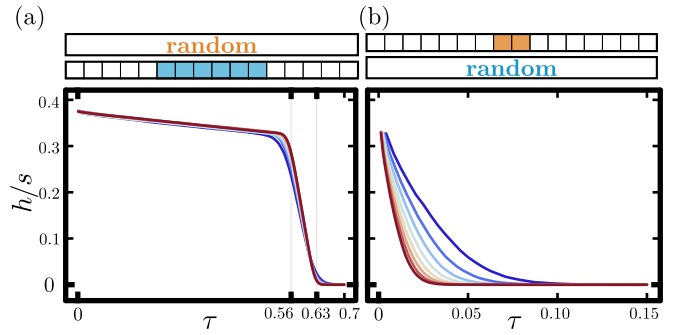


**FIG. S7.** Dynamics of  $h(\tau)$  under random selections of  $\mathcal{S}$  or  $\mathcal{M}$ . (a)  $\mathcal{S}$  is chosen randomly while  $\mathcal{M}$  is chosen consecutively. (b)  $\mathcal{M}$  is chosen randomly while  $\mathcal{S}$  is chosen consecutively.

DPTs depends on the boundaries of  $\mathcal{S}$ . We pick out qubits from the whole system randomly as  $\mathcal{S}$  with the size still fixed by  $s = \frac{2}{16}$ . Information now locate with various distance to the boundary of  $\mathcal{M}$ , thus the time at which they start to escape from both ends of  $\mathcal{M}$  distributes over a range of  $\tau$  values.

As shown in Fig. S7(a), when  $\mathcal{S}$  has no abrupt boundaries, the accelerate and the scrambled DPT point still exists. The scrambled point’s position is consistent with the prediction  $\tau_s(m) = \frac{m}{2}/v_1$  in the main text for  $m = \frac{6}{16}$ . The DPT points’ existence is thus independent on the boundary of information. Also note that the existence of  $\tau_a$  point demonstrates that it cannot be explained directly by the light-cone viewpoint of the quantum information propagation.

We also study the case when  $\mathcal{M}$  is chosen randomly, as shown in Fig. S7(b). At the thermodynamic limit  $N \rightarrow \infty$ , the normalized time  $\tau$  for the information to scramble over the system tends to  $\tau \rightarrow 0$ . This can be understood by rearranging the qubits to make  $\mathcal{M}$  consecutive and the resulting circuit would contain long-range random interactions. Thus, our results of the DPT points rely on consecutively selected measurement subsystem. For a generic chaotic system with long-range interactions, we expect it to be a fast-scrambler with no DPT exists in its evolution.

### DPTs in Quantum Information

When  $\mathcal{S}$  is contained in  $\mathcal{M}$ , as shown in Fig. S8(a),  $c = s$  before the  $\tau_e$  point. The position  $\tau_e(l) = l/v_1$  is consistent with that in the classical information model. The speed of decay accelerates also at the  $\tau_a$  point. At time  $\tau_s$ ,  $c$  turns from positive to negative, indicating that the amount of remaining quantum information turns to none. This is in agreement with the physical meaning of the scrambled point in classical information dynamics. At the last DPT point,  $c$  converges to its infinite-time limit  $-s$ . Consistent with the classical model for  $m > \frac{1}{2}$ , we denote it as the  $\tau_r$  point. This can also be understood from the perspective of the environment, in which the coherent information  $C^{\mathcal{E}} = -C^{\mathcal{M}}$  is fully recovered from its

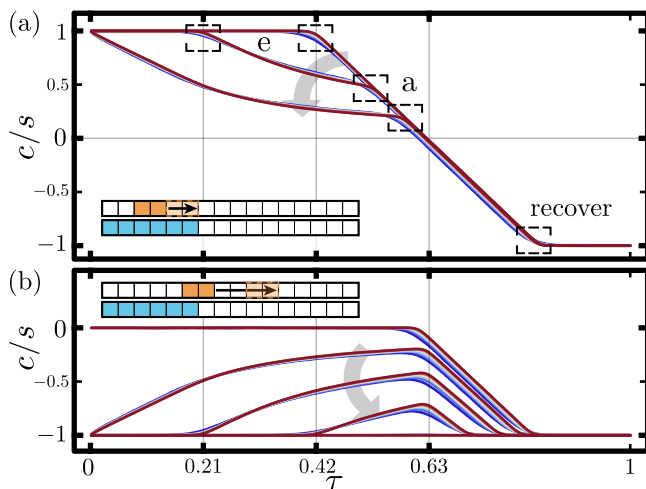


**FIG. S8.** Time evolution of average normalized coherent information  $c(\tau)$ . We again specify  $s = \frac{2}{16}$  and  $m = \frac{6}{16}$ .  $S$  is moved from the middle of  $\mathcal{M}$  to the outside, and the corresponding group of curves can be found from top to bottom. (a)  $S$  is contained in  $\mathcal{M}$ . Up to three DPT points can be observed which we denote as the  $\tau_e$ ,  $\tau_a$  and  $\tau_r$  point.  $\tau_r$  is the same for various selections of  $S$ . Additionally, there is a transition from positive to negative at the scrambled point  $\tau_s$  which consists with the classical information model. (b) Part of or all qubits in  $S$  are placed outside  $\mathcal{M}$ . The  $\tau_a$  points do not exist and the DPTs at  $\tau_s$  appears.

initially negative value. The  $\tau_r$  point is invariant when moving  $S$  inside  $\mathcal{M}$ .

As shown in Fig. S8(b), when half of  $S$  is placed inside  $\mathcal{M}$  and the other half is outside, the coherent information stays at zero until a DPT around  $\tau_s$ . When  $S$  is outside of  $\mathcal{M}$ ,  $c$  is initialized at its lower bound  $-s$ , indicating that all of the information are lost into  $\mathcal{E}$ . By definition,  $L$  here is the distance from the left boundary of  $S$  to the right boundary of  $\mathcal{M}$ . The  $\tau_e$  point where  $c$  starts to increase has again  $\tau_e(l) = l/v_1$ . This verifies its physical meaning that the light-cone of information reaches  $\mathcal{M}$  from either outside or inside.  $c$  increases until reaching maximum at the scrambled point. After  $\tau_s$ ,  $c$  decreases back to its lower bound until saturation through the  $\tau_r$  point.

\* zhuangjz21@mails.tsinghua.edu.cn

† lmduan@tsinghua.edu.cn

- [S1] J.-Z. Zhuang, Y.-K. Wu, and L.-M. Duan, Phase-transition-like behavior in information retrieval of a quantum scrambled random circuit system, *Phys. Rev. B* **106**, 144308 (2022).
- [S2] A. Nahum, S. Vijay, and J. Haah, Operator Spreading in Random Unitary Circuits, *Phys. Rev. X* **8**, 021014 (2018).
- [S3] A. Rényi, On measures of entropy and information, in *Proc. Fourth Berkeley Symp. Math. Stat. Probab. Vol. 1 Contrib. Theory Stat.*, Vol. 4 (University of California Press, 1961) pp. 547–562.